

ORIGINAL ARTICLE

In Vivo Identification of Thick, Thin, and Pale Stripes of Macaque Area V2 Using Submillimeter Resolution (f)MRI at 3 T

Xiaolian Li^{1,†}, Qi Zhu^{1,†}, Thomas Janssens^{1,4}, John T. Arsenault^{1,2}
and Wim Vanduffel^{1,2,3}

¹Laboratory of Neuro- and Psychophysiology, Department of Neurosciences, KU Leuven Medical School, Leuven 3000, Belgium, ²Athinoula A. Martinos Center for Biomedical Imaging, Massachusetts General Hospital, Charlestown, MA 02129, USA, ³Department of Radiology, Harvard Medical School, Boston, MA 02144, USA and ⁴Current address: Siemens Healthcare Belgium, Beersel 1654, Belgium

Address correspondence to Wim Vanduffel, KU Leuven, Lab. Neuro- and Psychophysiology, Campus Gasthuisberg, O&N 2, Herestraat 49-bus 1021, 3000 Leuven, Belgium. Email: wim@nmr.mgh.harvard.edu

[†]Contributed equally to the study.

Abstract

Primate area V2 contains a repetitive pattern of thick, thin and pale cytochrome oxidase stripes that are characterized by largely discrete in- and output channels, as well as differences in function, and myelo- and cytoarchitecture. Stripes have been identified mainly using microscope-based imaging of tiny portions of superficially located V2, or by postmortem methods, hence, the quest for (quasi) noninvasive tools to study these mesoscale functional units. Only recently, stripe-like V2 patterns have been demonstrated in humans with high-field (functional) magnetic resonance imaging (f)MRI, but in both such studies only 2 stripe compartments could be identified. Although interstripe distances in monkeys are ~half of those in humans, we show that all 3 V2 stripe classes can be reliably separated using submillimeter (f)MRI (0.6 mm isotropic voxels) on regular 3 T scanners by combining contrast agents and implanted phased-array coils. Specifically, we show highly reproducible fMRI patterns, both within and across subjects, of color-selective thin and disparity-selective thick stripes. Furthermore, reliable MRI-based higher myelin-density was observed in pale stripes. Hence, this is the first study showing segregation of columns using (f)MRI-based methods in macaque cortex, which opens the possibility of studying these elementary building blocks of the visual system noninvasively on a large scale.

Key words: color, columns, disparity, high-resolution fMRI, myelin

Introduction

Visual information is transmitted from retina to cortex through multiple parallel channels. Likewise, early visual cortical areas are characterized by subcompartments that can be differentiated based on their in- and outputs and the corresponding anatomical (cyto- and myeloarchitecture) and functional differences. These mesoscale functional compartments are oriented either parallel

(in layers) or orthogonal (in columns) to the cortical surface and allow partially segregated processing of, for example, color, orientation, disparity, and motion signals in the early visual stages. Since these mesoscale domains constitute essential building blocks of the visual system, it is crucial to understand their detailed functional architecture and interactions. However, techniques for studying mesoscale functional units on a larger scale

(i.e., throughout the cortex) have only recently been developed for primates.

In the second visual area (V2) of monkeys and humans, 3 column-like functional subdivisions have been described using cytochrome oxidase (CO) staining (Tootell et al. 1983; Horton 1984; DeYoe and Van Essen 1985; Hockfield et al. 1990): the CO-dark thin, CO-light pale (or inter), and CO-dark thick stripes. These stripes are typically organized in repetitive patterns as alternating thin-pale-thick-pale stripes, although variations exist (e.g., “thick pale thick pale” repetitions) (Roe et al. 2009). The individual stripe compartments are roughly 1–1.5 mm wide in macaque (Roe and Ts'o 1997), and approximately 1–3 mm in human (Hockfield et al. 1990). Furthermore, stripes of the same type are separated from one another by ~4 mm in macaque (Tootell and Hamilton 1989; Roe and Ts'o 1995, 1997; Lu et al. 2010) and 4–8 mm in human (Hockfield et al. 1990; Tootell and Taylor 1995). Double-label deoxyglucose (2L-DG), single-unit electrophysiology, and optical imaging studies showed that these CO-based subdivisions can also be characterized based on their functional properties, although the functional segregation is certainly not absolute (Peterhans and von der Heydt 1993; Levitt et al. 1994). Thin stripes contain more color- and luminance-selective cells, whereas thick stripes are more direction-, and disparity-selective, and the pale stripes are also selective for the axis of motion (Roe and Ts'o 1995; Vanduffel et al. 2002; Tootell et al. 2004; Chen et al. 2008; Roe et al. 2009; Lu et al. 2010; An et al. 2012; Nasr et al. 2016). In addition, some of the stripes typically contain higher myelin densities than the 2 other stripes (Krubitzer and Kaas 1989; Tootell and Taylor 1995). Since different staining methods for myelin can yield conflicting results (Horton and Hocking 1997), however, it remains unclear whether higher myelin densities should be attributed to pale, thick, or thin strips (Krubitzer and Kaas 1989; Tootell and Taylor 1995).

Most of our knowledge about the functional organization of V2-stripes has been gleaned from either a relatively small portion of V2 in living macaque monkeys, or from ex vivo studies. Indeed, although optical imaging and single-unit electrophysiology are well suited for studying V2 stripe function in vivo, optical imaging is restricted to the superficial layers of only the small part of (mainly dorsal) V2 in macaque monkeys not buried in the lunate sulcus (LS). Moreover, electrophysiology allows only a sparse sampling, and animals need to be sacrificed to confirm the recording sites postmortem. Similar issues hold true for 2L-DG, myelin or CO staining studies. Hence, there is a strong quest for tools to identify mesoscale functional units, methods which are less- or noninvasive and which allow investigations throughout the cortex in combination with follow-up studies in the same subjects. Although functional magnetic resonance imaging (fMRI) is a prime candidate for achieving this goal, V2 stripes remain difficult to isolate due to their small size.

Recently, however, an exquisite fMRI study using high-field scanners (7 T) with 1 mm isotropic voxels was able to identify 2 of the 3 stripe-types in human V2: color-selective thin stripes and disparity-selective thick stripes (Nasr et al. 2016). A second human imaging study at 7 T also showed a stripe-like pattern of activations based on motion sensitivity and differences in myelin content based on T1-weighted MRI contrasts (Dumoulin et al. 2017). These authors suggested that the higher myelin-density stripes corresponded to motion-sensitive thick stripes.

Identification of the various stripes in human V2 using (f)MRI relies on the assumption that they are characterized by the same functional and anatomical properties as those found in

nonhuman primates using invasive techniques. Validation, however, requires that the same properties be demonstrated in both human and nonhuman primates using the same method. Therefore, the goal of the present study is to use monkey fMRI to visualize the thin and thick stripes in vivo, and to further extend this approach to the third stripe type (pale). Unfortunately, the width (max 1.5 mm in macaques vs. 3 mm in humans) and distance between stripes of the same type (4 vs. 8 mm) are considerably smaller in macaques than humans, rendering our goal considerably more challenging, especially using commonly available low-field scanners (e.g. 3 T). To mitigate this problem, we scanned monkeys with submillimeter resolution using our recently developed implanted phased-array receive coils (Janssens et al. 2012). Although fMRI indirectly measures the neural activity based on the vascular response, previous studies in anaesthetized rats or cats have shown that submillimeter resolution fMRI based on the cerebral blood volume-weighted (CBV) signal yields excellent specificity and sensitivity for detecting neuronal activity in both columnar (Zhao et al. 2005; Fukuda et al. 2006) and laminar (Harel et al. 2006; Zhao et al. 2006; Poplawsky and Kim 2014; Poplawsky et al. 2015) cortical structures. In fact, it has been shown that blood-volume-dependent measures are better suited for segregating functional properties at mesoscale than conventional blood oxygenation-level dependent (BOLD) fMRI (Zhao et al. 2006; Kim and Kim 2010; Poplawsky et al. 2015). Nevertheless, mesoscale functional information of the brain has also been obtained using BOLD at high-field (Roe and Chen 2008; Yacoub et al. 2008; Zimmermann et al. 2011; De Martino et al. 2013; Wang et al. 2013; Muckli et al. 2015; Kemper et al. 2016; Reithler et al. 2017). Therefore, we also opted for contrast-agents in the present experiments (Vanduffel et al. 2001). The resolution of our functional scans (0.6 mm isotropic voxels) is approximately 1/4 to 1/16 that of the voxel volume typically used in monkey fMRI experiments, that is, 1–1.5 mm isotropic resolution (Zhu et al. 2012; Janssens et al. 2014; Yue et al. 2014; Chau et al. 2015; Liu et al. 2015; Russ et al. 2016; Miyamoto et al. 2017; Moeller et al. 2017; Sliwa and Freiwald 2017) and should be sufficient to visualize the functional architecture of column-like structures such as the V2 stripes, at least provided that we retain sufficient sensitivity using the combination of implanted coils and contrast agents.

In addition to the functional experiments, we proposed to study V2 stripes using in vivo myelin-density mapping (Glasser and Van Essen 2011; Chen et al. 2012; Sereno et al. 2013; Glasser et al. 2014; Fracasso et al. 2016). Since myelin contributes to most widely used MRI contrasts in brain research (T1, T2, T2*, proton density), MRI-based qualitative myelination mapping has been applied to investigate the macro-scale myelin content across the entire brain in humans and nonhuman primates. Moreover, a number of studies have shown that these maps correlate well with the cortical myelin content measured histologically (Geyer et al. 2011; Glasser and Van Essen 2011; Sereno et al. 2013; Glasser et al. 2014). However, in vivo visualization of finer-scale variations in myelin density has been attempted only in a very recent human study (Dumoulin et al. 2017). Here, we intended to exploit that feature using high-resolution (0.4 mm isotropic voxels) T1 weighted (T1-w) and T2 weighted (T2-w) MRI imaging and used the T1/T2 ratio proposed by Glasser et al. (2011,2014) as a proxy to identify in vivo variations in myelin-density (Glasser and Van Essen 2011; Glasser et al. 2014) within V2. Although it is only a relative rather than quantitative measure (Glasser and Van Essen 2011; Glasser et al. 2014), this approach provides a rather straightforward opportunity to

assess brain-wide variations in myelin-density within the same brain without systematic biases. By combining this myelination mapping with functional identification of 2 of the 3 stripes in V2 within the same subject, our results provided confirmative information about the exact stripe category with higher myelination examined with MRI. A sequence-dependent limitation forced us to acquire 0.6 mm isotropic data only from a restricted portion of the brain. We decided to focus on the dorsal 50–60% of the cerebrum, where the temporal signal-to-noise ratio (tSNR) was also higher compared with ventral regions due to the geometry of the coils. Further technological improvements may include an increase in the number of channels of the implanted phased-array coil, thereby covering regions more ventrally, or the application of the same technology at higher magnetic fields (7 T and higher). Such developments will undoubtedly improve the detectability and characterization of mesoscale functional units throughout the cortex.

Materials and Methods

Subjects

Three rhesus monkeys (*Macaca mulatta*; 1 female; 4–7 kg) were subjects in this study. They were implanted with 8 (M1 and M2) or 7 (M3) channel phased-array receive coils embedded in an MRI-compatible headpost to improve the sensitivity of high-resolution (f)MRI (Janssens et al. 2012). The monkeys were trained to maintain fixation while they were constrained by headposts in a natural “sphinx” position inside a plastic box. Immediately before the fMRI scan, monocrySTALLINE iron oxide nanoparticle (MION, Feraheme, AMAG Pharmaceuticals; 8–11 mg/kg) was injected into the femoral/saphenous vein of the animals to improve the contrast-to-noise ratio (CNR) and to avoid the influence of superficial draining veins (Vanduffel et al. 2001). Subject M3 participated only in the color-selective thin stripe visualization and retinotopy mapping experiments, as this animal had to be euthanized because of an unrelated pathology (untreatable severe lower back disk herniation).

Animal care and experimental procedures were performed in accordance with the National Institute of Health’s Guide for the Care and Use of Laboratory Animal, the European legislation (Directive 2010/63/EU) and were approved by the Ethical Committee of KU Leuven. Animal housing and handling were according to the recommendations of the Weatherall report, allowing extensive locomotor behavior, social interactions and foraging. All animals were group-housed (cage size at least 16–32 m³) with cage enrichment (toys, foraging devices) at the primate facility of the KU Leuven Medical School.

Imaging

fMRI

fMRI scans were performed on a 3 T Siemens PRISMA scanner for all experiments using subject M1 and for the thick stripe experiment of M2. High-resolution (0.6 mm isotropic voxel size) T2* weighted echo planar images (EPI) covering the whole brain were collected using a simultaneous multiple slice (SMS) (Nunes et al. 2006; Xu et al. 2013; Kim et al. 2016) EPI sequence (repetition time [TR] = 3000 ms, echo time [TE] = 22 ms, accelerated multiband [MB] = 2, acceleration factor = 3, flip angle [α] = 90°, matrix size 140 × 140 × 74). All other experiments (of subjects M2 and M3) were conducted on a 3 T Siemens TIM TRIO scanner with a AC88 gradient insert. High-resolution (0.6 mm isotropic voxel size) T2* weighted EPI images were collected

using a standard EPI sequence (TR = 3000 ms, TE = 21 ms, acceleration factor = 2, α = 90°, matrix size 140 × 140 × 48). Only the upper halves of the brains were covered due to a limited number of slices that could be scanned using this sequence.

Myelin-Density Maps

High-resolution (0.4 mm isotropic voxel size) T1-w and T2-w images were acquired on the 3 T Siemens PRISMA scanner for subjects M1 and M2, to create myelin density maps (Glasser and Van Essen 2011). They were scanned under ketamine–xylazine anesthesia, using a single-loop receive coil and the body transmitter from the scanner. During one scan session, 11 and 7 T1-w images were acquired for subjects M1 and M2, respectively, with a magnetization prepared rapid gradient echo (MPRAGE) sequence (TR = 2700 ms, TE = 3.5 ms, α = 9°, inversion time [TI] = 882 ms, matrix size 320 × 260 × 208). For subject M1/M2, 5/4 T2-w images were acquired using a “sampling perfection with application optimized contrasts using different flip angle evolution” (SPACE) sequence (TR = 3200 ms, TE = 456 ms, variable α , matrix size 320 × 260 × 208, Turbo Factor = 131, echo spacing = 6 ms).

Reference Anatomical Image

We repurposed the T1-w images used for the myelin density maps as a reference anatomical image for M1. For subject M2 and M3, the reference structural data were acquired in a separate session before the start of all other experiments. 12/15 high-resolution T1-w (0.4 mm isotropic voxel size, TR = 2500 ms, TE = 4.35 ms, α = 9°, TI = 850 ms, matrix size 320 × 260 × 208) images were acquired on the 3 T Siemens TIM TRIO scanner using a single-loop receive coil and the standard body transmit coil while the subjects were under ketamine–xylazine anesthesia. To achieve a better registration of the EPIs to the reference anatomical image, we acquired T1-w 3D gradient echo (GRE) images (0.6 mm isotropic voxel size, TR = 6 ms, TE = 2.63 ms, α = 11°, matrix size 160 × 160 × 96) in every fMRI session, as an intermediate image for the registration.

Field Maps

High-resolution field maps which contained 2 images with different TE (0.6 × 0.6 × 0.7 mm voxel size, TR = 917 ms, TE₁ = 6.48 ms, TE₂ = 8.94 ms, α = 55°, matrix size 140 × 140 × 66) were collected from the 3 T Siemens PRISMA scanner for subjects M1 and M2 during a separate session under anesthesia. These images were used to correct for EPI distortions caused by magnetic field inhomogeneity for experiments conducted on the same scanner from these 2 subjects.

Visual Stimuli and Experimental Design

A Barco LCD projector was used to project the stimuli at 1400 × 1050 resolution and 60 Hz refresh rate onto a translucent screen located 57 cm from the monkey’s eyes. Eye movements were monitored using an eye-tracking system based on infrared corneal reflection (ISCAN). Only runs in which the subjects maintained fixation on a small square-shape target within a fixation window (2° × 2°) in the center of the stimulus for more than 90% of the time were used for further analysis.

Experiment 1

Thin (color-selective) stripes: Circular moving radial grating stimuli (Fig. 1A,B) similar to those used in our previous double-label deoxyglucose (2 L-DG) study (Tootell et al. 2004) were employed

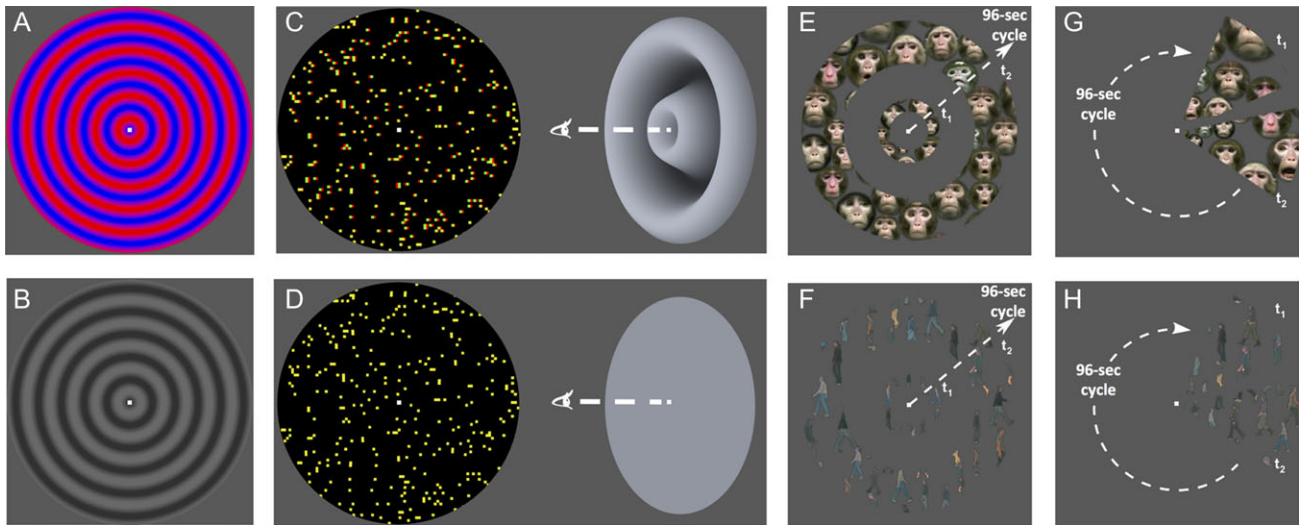


Figure 1. Exemplars of stimuli used in all the experiments. (A and B) Isoluminant color and achromatic radial grating stimuli used as the thin-stripe localizer. (C and D) Stimuli used for thick-stripe localizer. Red/green and yellow anaglyphs in the left panel are disparity stimuli and their monocular counterparts. The 3D renderings next to them show their perceived depth structures. (E–H) Retinotopic mapping stimuli. Adapted with permission from Janssens et al. (2014). (E) and (F) are moving annuli used to map eccentricity. (G) and (H) are rotating wedges used to map polar angle. Animated monkey faces (top) or walking humans (bottom) were shown within the rings or wedges.

to selectively activate V2 color-selective thin stripes. The sizes of the color-varying and luminance-varying stimuli were identical (diameter = 24.5° of visual angle), and their mean luminances were both adjusted to 17.4 cd/m^2 to equalize the cone excitation ratios across stimuli. The equiluminant color-varying gratings varied between equiluminant red-blue values for macaque (red to blue luminance ratio = 6) (Tootell et al. 2004). The waveform of the grating was trapezoidal in shape, so that the square-wave component could give optimal contrast at each stimulated location and the sine-wave component could eliminate aberration at the edges between different colors. According to a macaque physiology study (Thorell et al. 1984), the sensitivity to color is higher than to luminance at a lower spatial frequencies, therefore, we chose a low spatial frequency grating (0.45 cycles/degree).

A block design was conducted and each block lasted 30 s (M1) or 18 s (M2 and M3) during which one of the moving gratings was presented with a speed of 0.52 cycles/s. The moving direction was centrifugal during the first half of each block, and centripetal during the last half of the block. Blank blocks in which only a uniform gray background was presented were used at the beginning of each run to allow the MION signal to reach equilibrium. The color and achromatic stimulus blocks were presented in an alternating order. For subject M1, blank blocks were also presented between each color and achromatic stimulus blocks. Data from 2 scan sessions were acquired in different days for M1 and M2 (9 or 10 runs per session for M1 and 22 runs per session for M2) and 1 session in 1 day for M3 (21 runs in total). Each run lasted for 627 or 765 s, containing 209 or 255 volumes.

Experiment 2

Thick (disparity-selective) stripes: Size-matched disparity-defined 3D radial sinusoidal gratings and their monocular counterparts were used as stimuli (Fig. 1C,D). The disparity stimulus was defined by random dot stereograms with 5% density red and green dots depicting each view of the 3D grating. The depth of the grating varied from near 0.22° to far 0.22° relative to the

frontoparallel plane. Subjects wore red–green spectacles to perceive the depth. Two monocular stimuli were created from either the red or green dots of the disparity stimulus, and the color was set to the same yellow shade as the disparity stimulus seen through the goggles. The same image was presented to both eyes for the monocular stimuli, hence no disparity was present. Two gratings were used for the disparity stimuli for subject M2, one with a spatial frequency matched to the color stimuli (0.45 cycles/degree) and another with a lower spatial frequency (0.16 cycles/degree). As it had proved to be more efficient in experiments using M2, only the lower spatial frequency stimuli were used for subject M1. Each block lasted 30 s during which the grating was presented at a speed of 0.52 cycles/s, with the direction reversed in the middle of each block. Blank blocks were presented at the beginning of each run and between each binocular and monocular block. Data from 2 scan sessions (10 or 17 runs per session) were acquired on different days for subject M1 and 7 sessions (6–8 runs per session) on different days for subject M2. Each run lasted for 765 s, containing 255 functional volumes.

Retinotopic Mapping Experiment

We used the stimuli from one of our previous studies (Janssens et al. 2014). Dilating or contracting annuli and wedges rotating clockwise or counter-clockwise, traversing the area between 0.25° and 12.25° of visual angle in radius, were used to drive phase-locked activations for calculating polar angle and eccentricity maps independently. We used both the dilating and contracting annuli, and both the clockwise and counter-clockwise wedges to cancel phase errors caused by hemodynamic response lags. All wedges, and the largest annuli, measured 12.25° in radius, so that their size was matched to the stripe-localizer experiments. Dynamic monkey faces (Zhu et al. 2012) and walking humans were confined to the annuli and wedges. Each cycle lasted 96 s and each run contained 4 cycles. Subject M1 was scanned for 3 sessions with the whole brain covered. Subjects M2 and M3 were scanned for 4 and 5 sessions,

respectively, but the slices covered only the top part of the brain. From 13 to 32 runs of data were acquired in each session.

Data Analysis

fMRI Image Reconstruction and Preprocessing

The EPI images were reconstructed using an “optimized generalized autocalibrating partially parallel acquisitions” (GRAPPA) reconstruction method (Hoge and Polimeni 2015) to decrease artefacts caused by the movements of the monkeys.

The preprocessing was performed using Freesurfer (<http://surfer.nmr.mgh.harvard.edu>) and Bioimage suite (<http://bioimagesuite.yale.edu>). The EPI images were masked to remove nonbrain signals. This was followed by motion correction using one EPI volume as the template. The template was one EPI image acquired during the separate field map scanning session for experiments conducted on the Prisma scanner from subjects M1 and M2. For experiments conducted on the Tim Trio scanner from subject M2 and M3, the single, best EPI image chosen from the best run, during which the monkeys scarcely moved was used as the template. Finally, similar to our previous studies (Kolster et al. 2009), a slice-by-slice undistortion correction was performed according to the same template using a B-spline grid-based nonlinear registration method to reduce frame-to-frame distortions.

GLM Analysis

For the stripe-localizer experiments, a general linear model (GLM) analysis was performed in Freesurfer to calculate percent signal changes and t-score maps. A GLM denoising algorithm (Kay et al. 2013) was used to generate noise regressors using signals from white matter and ventricles, thereby reducing physiological and other nuisance temporal domain noises caused by monkey body motion. Condition regressors were generated by convolving the predictors by a canonical gamma fit impulse response function (IRF) for the MION signal (Vanduffel et al. 2001; Leite et al. 2002). The first 4 dummy scans of each run were acquired to allow the scanner to reach equilibrium, and thus were excluded from the GLM analysis. To account for low-frequency scanner signal drifts, both linear and quadratic regressors centered around zero were included as additional factors in the GLM model. The mean fixation performance of the analyzed runs exceeded 94% of the run duration (Supplementary Table S1), therefore, no further regressors based on fixation performance were used during the statistical analysis of the data.

For the retinotopic mapping experiment, polar angle, eccentricity, and field-sign maps were calculated following the procedure described by Sereno et al. (1995) using Freesurfer. Nuisance regressors for the GLM analysis included 3 principle components derived from 6 motion-correction parameters and the linear and quadratic trend removals.

Registration From EPI to Structure Data and Surface Projection

The results of the GLM analyses (e.g., t-score or retinotopic maps) in the 3D volume were registered to the reference anatomical images through an intermediate 3D GRE image acquired in the same session as the EPI template. The results were then projected onto the surface. For the retinotopy and thin stripe experiments of subjects M2 and M3, the EPI and GRE images were acquired with a gradient coil (the AC88 insert) differing from the reference anatomical images (which were acquired using the standard scanner gradient coil). A gradient distortion correction (Jovicich et al. 2006) was performed on these EPI and GRE images to correct for image distortions due to nonlinearity

of the magnetic fields from different gradient coils. A 1D non-linear registration along the phase-encoding direction was then performed to correct for EPI distortions relative to the GRE images using JIP toolkit provided by Joseph Mandeville (<http://www.nitrc.org/projects/jip>), since the field maps acquired for these experiments were contaminated by susceptibility artefacts. For all data from subject M1 and for the data of the thick stripe experiment from subject M2, a fieldmap-based EPI distortion correction (Jezzard and Balaban 1995) was performed using FSL (Jenkinson et al. 2012), to achieve better alignment between functional and structural data. The final results were projected onto the surface, and activations located between 20% and 80% of the cortical depth (between the gray–white matter boundary and pial surface) were sampled in steps of 10% and averaged to create the surface maps. This procedure minimizes the effects of cerebrospinal fluid (CSF), white matter and pial vein signals on the activations, and reduces the cross-talk between superficial layers in the 2 banks of neighboring surfaces within the same sulcus (Glasser et al. 2013). No extra spatial smoothing was applied on the volume data. Heat kernel smoothing (bandwidth = 1, iteration = 1) (Chung et al. 2008) was applied on surface data. Iso-t-score contour lines were drawn based on the smoothed t-scores along the surface (see left panel of Fig. 3, colored lines).

Isolation of Stripes Based on fMRI Activations

Activations originating from V2 stripes of the same kind were isolated using a custom-designed algorithm based on thresholded iso-t-score lines (P -value < 0.05). Activations with different local maxima were separated into different clusters. The extension of each cluster was defined by a waterfall algorithm starting from the peak, either until it reached the first local minimum contour level surrounding the peak, or until it reached the threshold (Fig. 3, right panel). Clusters so defined were used to represent functionally defined V2 thin (color-selective) and thick (disparity-selective) stripes.

Anatomical Image Segmentation

Reference anatomical images were created by averaging all T1-w images from the same session to improve SNR. Image segmentation and surface creation were performed in Freesurfer (Dale et al. 1999; Fischl, Sereno, and Dale 1999) following a procedure similar to that described for humans.

Myelin-Density Maps

We followed the pipeline from Caret (Van Essen et al. 2001; Glasser and Van Essen 2011) (<http://www.nitrc.org/projects/caret/>) for the myelin density mapping analysis. As the T1-w and T2-w images were collected during the same session under anesthesia, the ratio between T1-w and T2-w images could be calculated without any registration or motion correction. Several T1-w or T2-w images were averaged to improve image SNR. Surfaces and gray-matter ribbons were created from the same averaged T1-w images using Freesurfer and imported into Caret for the myelin-density mapping analysis. Only voxels in the gray matter ribbon centered between the pial and white matter surfaces were selected for the analysis to avoid partial volume effects caused by pial, CSF or white matter intrusion. To remove the effect of improper segmentation of CSF or veins, outliers were defined as those voxels that exceeded one standard deviation of the T1/T2 ratio in cylinders orthogonal to the surface with the same height and radius as the cortical thickness. The volume-to-surface projection of the T1/T2 ratio was performed using a Gaussian weighted function.

Outlier vertices were further detected and removed on the surface by including only vertices with T1/T2 ratios less than 4 standard deviations from the mean T1/T2 ratio from all the vertices within 10 vertices of them. The value of each vertex outlier was replaced with a Gaussian-weighted average T1/T2 ratio of its neighboring vertices. High spatial frequency noise was finally removed by applying one iteration of Gaussian smoothing (strength = 1) on the resulting myelin maps.

For subject M2, since the reference anatomical image was a different average T1-w image acquired before the myelination scans, we used surface-to-surface registration based on cortical folding structures (Fischl, Sereno, Tootell, et al. 1999) to register myelin maps to the template surface created from the reference anatomical image.

The myelin maps from both subjects were displayed using a threshold between 0% and 80% percentile values to visualize the more heavily myelinated stripes more clearly.

Reliability Test

Test-retest correlation analyses were conducted on color-, disparity-selective activations, and myelin maps in dorsal V2 (V2d) to quantify the reliability of the results. To achieve a more rigorous test, fMRI data acquired on different days for subjects M1 and M2 were assigned to different test sets. Only for subject M3 were data collected during a single session, hence they were split into odd and even runs. The same approach was used for myelin maps from all subjects. Data were reanalyzed for test and retest data sets independently and a Spearman correlation coefficient was calculated between the results from the 2 sets for each experiment and subject separately. To reduce statistical bias introduced by intrinsic correlation between neighboring cortical vertices, a stricter permutation test as proposed by Nasr et al. (2016) was also conducted. In this analysis, 10% of the vertices in V2d were randomly selected each time, and the correlation between different sets was compared with the correlation of 10% spatially randomly shuffled V2d vertices between different sets. The same procedure was repeated 100 000 times and *P*-values were calculated based on the probability that the correlation between test and retest sets in aligned vertices was smaller than in randomly shuffled vertices.

Quantitative Test for Higher Myelination in Pale Stripes

To quantitatively confirm that neither the functionally defined thin nor thick stripes overlap with the heavily myelinated stripes, we performed a permutation test combining the data from the 2 hemispheres of each animal. In the permutation test for each functionally defined stripe type (thin or thick stripes), we calculated the probability that the median myelin density in these stripes were to be higher than the median density from randomly selected vertices (keeping the number of vertices equal to those in the thick or thin stripes) throughout V2d across 100 000 permutations. The median value was calculated, since myelin density values across V2d are not normally distributed (Jarque-Bera test). To avoid the effect of the thick stripe vertices in the permutation test of the thin stripes, we randomly selected vertices throughout V2d excluding the thick stripe vertices. Likewise, for the permutation test of the thick stripes, thin stripe vertices were excluded from the random vertex selection. Thus, we compared myelin densities in each type of functionally defined stripe with the myelin density from the same stripe compartment plus the pale stripes in each permutation test.

Note that T2* signals, the source of EPI image intensity, are theoretically negatively correlated with myelin density (Li et al. 2009; Chen et al. 2012). Therefore, it is possible that the tSNR in color and disparity experiments inversely covaries with myelin density and thus bias the above permutation test. To check this, we ran similar permutation tests and compared median tSNR in V2d vertices excluding thin and thick stripes with the randomly selected vertices (keeping the number of vertices equal to those outside the thin and thick stripes) throughout V2d for both the color and disparity experiments separately. The tSNR was calculated for each voxel in the GLM analysis as average image intensity across frames after removing the task and nuisance regressors and divided by the temporal standard deviation. Since only vertices with reliable tSNR were meaningful for such tests, vertices with tSNR lower than the 15th percentile within V2d were excluded from the analysis.

To rule out the possibility that tSNR differences caused the colocalization of color and disparity stripes in lower myelinated areas in the permutation test results, we conducted a further nonparametric paired test (Wilcoxon signed-rank test) analysis in which tSNR across the 3 types of stripes was tightly controlled for. To do so, vertices within V2d were divided into 10 equally spaced tSNR bands for each experiment (color or disparity) after vertices with tSNR lower than the 15th percentile were excluded. For the color data, 2 median values were calculated for each tSNR band corresponding to median myelin density in thin and vertices including pale stripes (all V2d vertices that excluded the thin and thick stripes) and were compared using Wilcoxon signed-rank test across all the tSNR bands, hemispheres, and subjects. Myelin densities throughout V2d in each subject were converted to percentiles before median values were calculated to allow pooling of the values across subjects (Glasser and Van Essen 2011; Glasser et al. 2014). For the disparity data, median myelin density in thick and vertices including pale stripes were calculated and compared. Since for each type of stripes in each hemisphere of each subject, 10 median values were calculated from 10 tSNR bands, in total 40 median values were pooled together for each type of stripes for the Wilcoxon signed-rank test. Note that a subject random effect analysis cannot be used for the Wilcoxon signed rank tests, therefore, a fixed effect analysis was performed.

Results

Retinotopic Delineation of V2d

We used retinotopic mapping to delineate the V2 boundaries in each hemisphere of each monkey independently from the stripe-visualization experiments. Figure 2 shows the retinotopy of the left hemisphere for a representative subject. Since ventral V2 was not fully covered in 2 of 3 subjects and because of the lower sensitivity due to the specific configuration of the implant coil in the third animal, we focused only on V2d. The polar angle map (Fig. 2A,D) shows a mirror-reversal of the retinotopic organization in V2d compared with V1. In Figure 2C,F, this mirror-reversal was represented as a different field sign in V2d compared with V1 (red vs. blue). The caudal border of V2d was designated as a transition of the field sign (black solid lines in Fig. 2). This border was located along the posterior lip of the LS, and matches the reported anatomical location of the V1/V2d border (Gattass et al. 1981; Roe and Ts'o 1997; Lyon et al. 2014). The retinotopic definition of the rostral border of V2d is less straightforward in macaque monkeys, since a noncontinuous retinotopic organization has been reported immediately

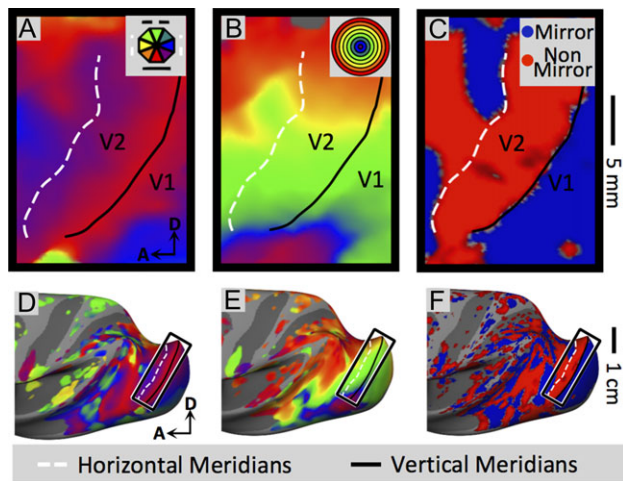


Figure 2. Retinotopic results from the left hemisphere of a typical subject (M2). The figures from left to right show polar angle (A and D), eccentricity (B and E) and field sign (C and F) maps on inflated (D–F) and flattened (A–C) surfaces separately. The enlarged dorsal parts of the extrastriate cortex in A–C are highlighted by black rectangles in (D–F). The colors in (A, B, D, and E) represent phase information of the polar angles and eccentricities. In the legend of (B), the colors from central to peripheral representations correspond to eccentricities ranging from: 0.25–0.41, 0.41–0.66, 0.66–1.08, 1.08–1.75, 1.75–2.85, 2.85–4.63, 4.63–7.53, and 7.53–12.25 degrees. All maps are thresholded at P -values < 0.05 .

rostral to V2d (Gattass et al. 1988). This discontinuity, which is often reported in New World monkey studies (Rosa and Tweedale 2000; Rosa et al. 2005, 2009, 2013, Jeffs et al. 2009, 2013; Sereno et al. 2015), was also observed in our results, and is apparent as a red extension of the field sign map in the rostral direction (Fig. 2C,F). Although multiple visual-field map models have been proposed, explaining the regional topographic organization anterior to V2d (Angelucci and Rosa 2015; Gattass et al. 2015; Jeffs et al. 2015; Kaas et al. 2015), all these models define the rostral V2d border as a continuous line following the field sign map reversals presented along most of that border to have similar width of V2d throughout the whole region. The same criterion was used here (see white dashed lines in Fig. 2). Note that due to partial volume effects, a horizontal meridian can have a nonzero phase value in cases where the visual field representation does not cross the horizontal meridian (i.e., for quadrant instead of hemifield representations). This is the case for the visual field representations in V2d and its neighboring regions. Therefore, the V2d borders were mainly based on field sign reversals, as shown in Figure 2C, and since field signs are determined only by the angle between the direction of the gradients in eccentricity and polar angle thus are not biased by partial volume effects.

Experiment 1

Thin (Color-Selective) Stripes

After identifying the V2d borders, we examined whether color-selective activations showed a consistent stripe-like pattern in V2d across all hemispheres. Activations evoked by isoluminant color-varying stimuli were contrasted with luminance-varying achromatic stimuli to determine color-selective activations. Figure 3 shows the V2d color activation on the flattened surface of the right hemisphere of subject M1. The black solid line indicates the V2d border as defined by the retinotopic mapping. Iso-t-score lines were drawn overlying the activations to help distinguish separate clusters of high color-selectivity. As color-

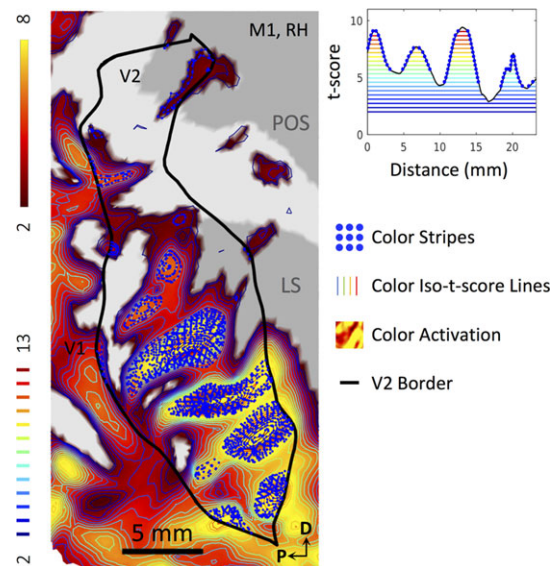


Figure 3. Isolation of thin stripes based on color-selective activations. Color-selective activation from the right hemisphere of subject M1 is shown. The colored contour lines overlying the activation map are iso-t-score lines generated based on the activation. The right panel plot shows the same activation along a line drawn through the middle of V2 from the central to periphery and the iso-t-score lines are simplified as colored horizontal lines. Identified high-activation clusters, which represent functionally defined V2 thin stripes, are identified based on the highest saddles around them and are indicated by blue dots. Black outline indicates the border of retinotopically defined V2. RH, right hemisphere; LS, lunete sulcus; POS, parieto-occipital sulcus.

selective activations should be strongest in color-selective thin stripes and weaker in other stripes, these high-activity clusters most likely represent thin stripes. The clusters were isolated based on iso-t-score lines, using the waterfall method illustrated in the right upper panel of Figure 3 (see also Materials and Methods). More specifically, high-activity clusters were demarcated at the level of the first local minimum (or the saddle point) surrounding the peaks. To better visualize the separate stripes, the isolated peaks were marked by blue dots.

As shown in Figure 3, several stripes with strong color-selectivity ran perpendicularly to the retinotopically defined V1/V2 border across the entire width of V2d, forming an alternating pattern of stripe-like activations. This pattern is particularly prominent after separating peak activations by the blue dots using the waterfall-isolation method (see top right inset in Fig. 3). This banded activation pattern fits well with the features described for V2 thin stripes (Tootell et al. 1983, 2004). Similar results were observed in all hemispheres of our 3 subjects (Fig. 4).

To test the reproducibility of these stripes, we co-registered the color stripes (blue dots) defined by a test data set (half of the sessions across days for subjects M1 and M2 and odd runs for subject M3) to the color activation of a retest data set (the other half of the sessions for subjects M1 and M2 and even runs for subject M3) (Fig. 5). All the blue dots (test data) are found at exactly the same location as the peak activations of the retest data. This banded pattern is consistent across sessions in all 3 monkeys, showing qualitatively its reliability and reproducibility. To further quantify their consistency, we calculated Spearman correlation coefficients for percent signal change in color-selective activations in V2d between the test and retest data sets for each hemisphere and each subject. All correlation coefficients are very high ($r_s > 0.55$) (Table 1). The

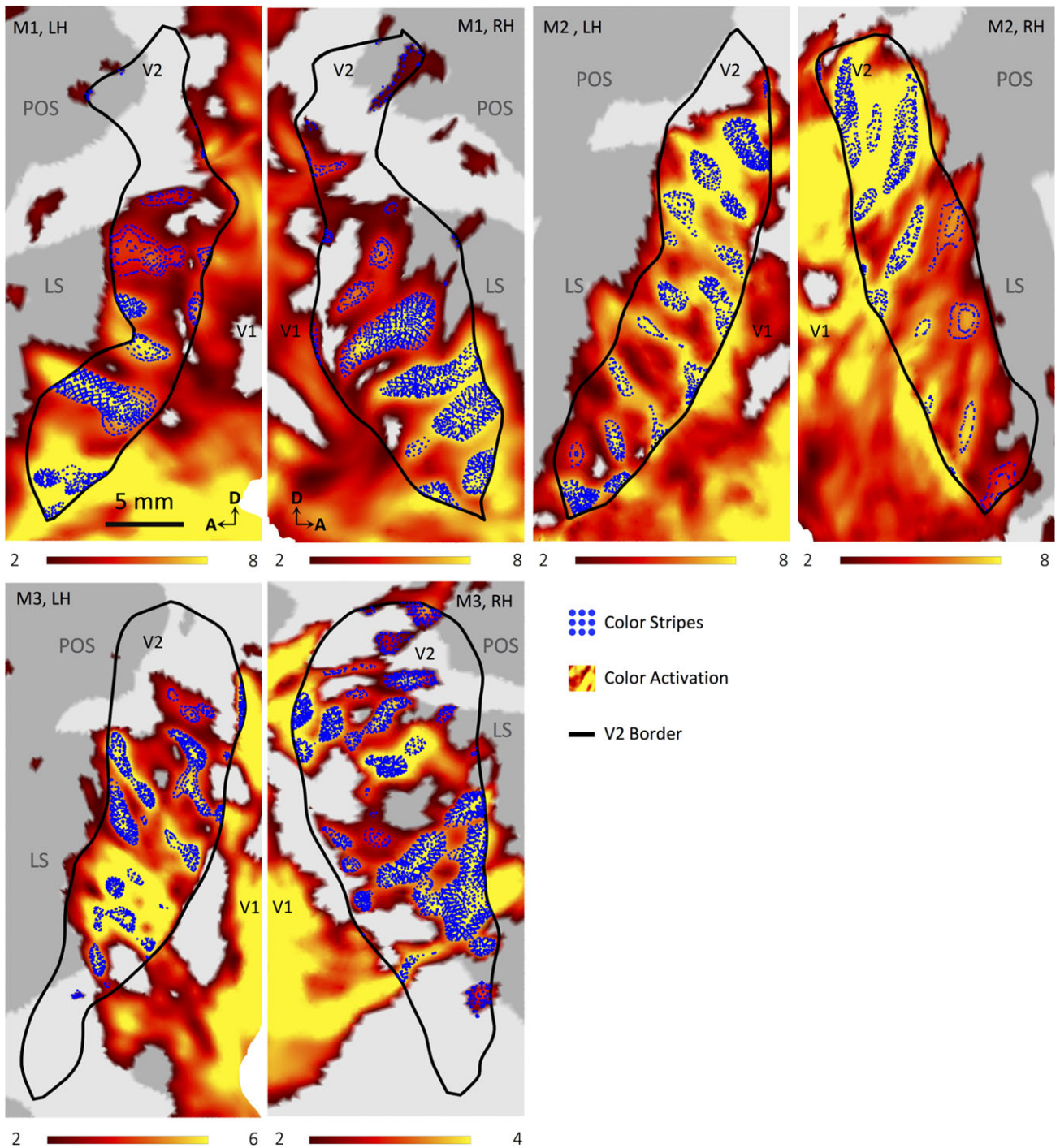


Figure 4. Color-selective activation maps in all hemispheres. The V2 thin (color-selective) stripes are marked by blue dots. Black outline, retinotopically defined V2; LH, left hemisphere; RH, right hemisphere. The scale bar is for all panels.

P-values are also highly significant for all correlation coefficients. However, since all the V2d vertices were included, and due to the intrinsic correlation in percent signal changes between neighboring cortical vertices, the standard errors are underestimated and introduce a bias in the P-values. To overcome this bias, we performed a permutation test as proposed by Nasr et al. (2016) (see Materials and Methods). All the P-values from the permutation test from all the hemispheres are smaller than 10^{-5} . This indicates high reliability for the

observed color-selective activation bands across the entire extent of V2d in all hemispheres.

Experiment 2

Thick (Disparity-Selective) Stripes and Their Relationship to the Thin Stripes

Disparity-selective activations were generated by contrasting 3D radial sine-wave gratings with their monocular counterparts.

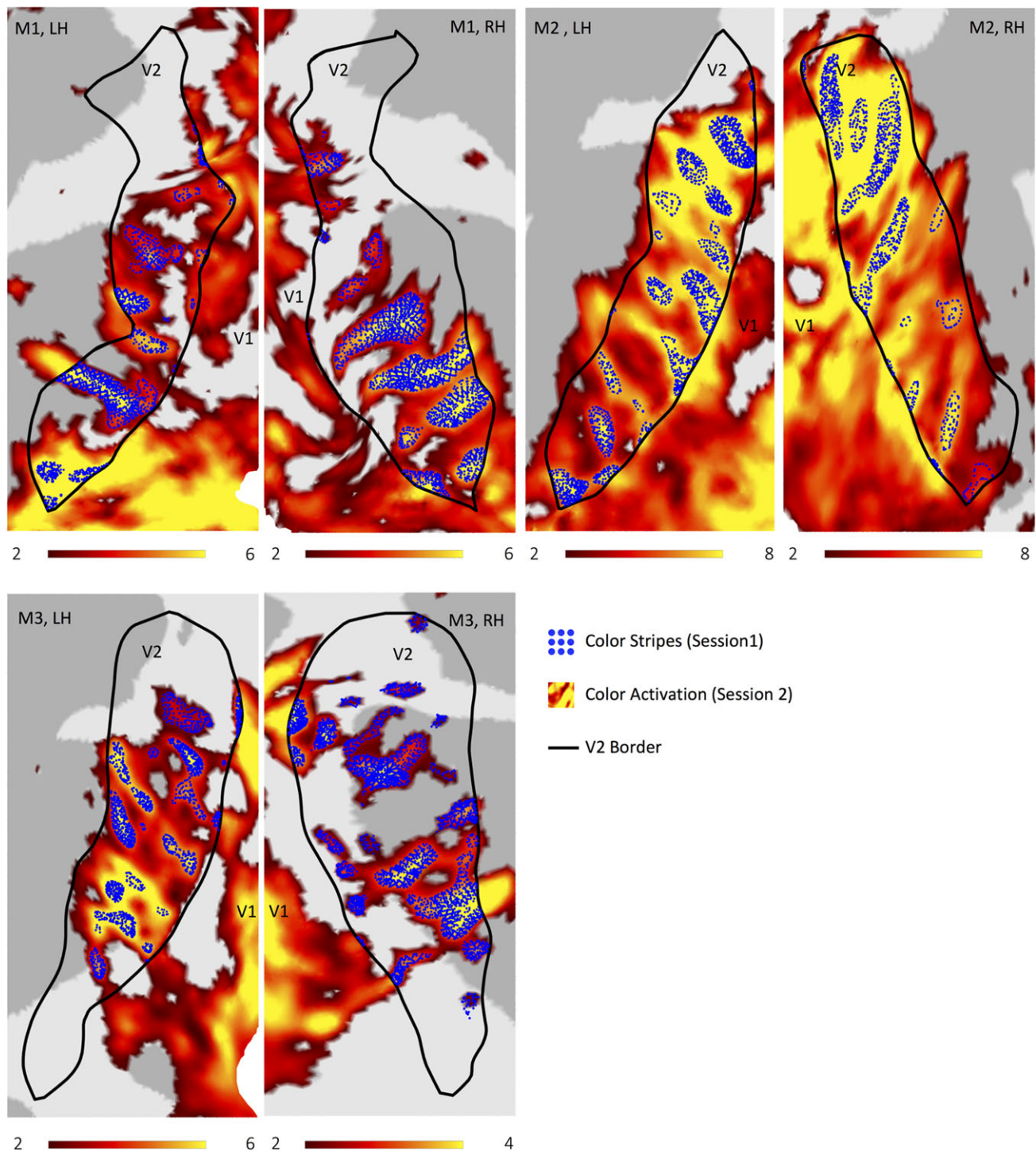


Figure 5. Reproducibility of color-selective activations across different sessions. The V2 thin (color-selective) stripes from test session(s) (marked by blue dots) are shown on top of color-selective activation maps from retest session(s). Other details as in Figure 4.

The results are shown in Figure 6 (upper panels). The green dots indicate the higher activations, using a procedure similar to that described for the color-selective thin strips (above), and represent the locations of disparity-selective thick stripes. As with the color-selective activations in V2d, these disparity-selective activations form a banded pattern oriented perpendicular to the V2d border spanning almost the entire width of V2d in both hemispheres of both subjects. The disparity-selective

activations are also highly reproducible: the intersession test-retest Spearman correlation coefficients of the percentage signal changes (disparity versus monocular stimuli) are high ($r_s > 0.46$), and statistically significant (P -values $< 10^{-5}$, permutation test) (Table 1).

The next question is whether these presumptive thick disparity stripes are located at positions differing from the thin color stripes, as one would predict from previous optical

Table 1 Reliability test results

	Color	Disparity	Myelination
M1			
LH	0.58*	0.93*	0.96*
RH	0.77*	0.83*	0.93*
M2			
LH	0.62*	0.51*	0.89*
RH	0.55*	0.46*	0.94*
M3			
LH	0.91*	N.A.	N.A.
RH	0.80*	N.A.	N.A.

*All of them are highly significant ($P < 10^{-5}$).

Table 2 Spearman correlation coefficients between color and disparity activations in V2d

M1	LH	-0.23*
	RH	-0.46*
M2	LH	-0.60*
	RH	-0.41*

*All of them are highly significant ($P < 10^{-5}$).

imaging and CO staining studies (Tootell et al. 1983; Chen et al. 2008). To answer this question, we coregistered the color-selective thin stripes with the disparity-selective thick stripes in V2d (Fig. 6, lower panels). They appeared to be largely separated from each other, with the color-selective stripes (blue dots) largely interspersed between these disparity-selective activations. The same interdigitating activation pattern was found in all 4 hemispheres. To further quantify the nature of this interleaved pattern, we calculated the correlation coefficient of the percent signal changes between color and disparity activations (Table 2). To avoid the effect of interstripes, which are not color or disparity selective, or regions with lower SNR, we calculated the correlation across the voxels identified as thin and thick stripes. We found a significantly negative correlation ($r_s < -0.23$, permutation test P -values $< 10^{-5}$) between color and disparity activations, indicative of their distinct identities.

Experiment 3

Interstripes or Pale Stripes (Heavier Myelination)

The T1/T2 ratio has been used as a measure of variations in myelin density throughout the brain. Because it provides relative rather than quantitative myelination information (Glaser and Van Essen 2011; Glasser et al., 2014), the T1/T2 ratio was only compared within the same brain, rather than across subjects. Consistent with previous studies, stronger myelination was observed in multiple regions including primary visual cortex, middle temporal areas (MT), primary auditory, and somatosensory cortex (Glasser and Van Essen 2011; Glasser et al. 2014; De Martino et al. 2015). At mesoscale, the higher myelinated layer IV in V1 (band of Gennari) is also clearly visible, while no layer-specific variations were obvious in V2 (Supplementary Fig. S1). This result suggests that the T1/T2 ratio can be used to detect mesoscale variations in myelin-density, also at the level of V2 stripes.

In V2d, a stripe-like pattern of regions alternating between higher and lower myelin densities was observed. Exactly as with color- and disparity-selective stripes, the high-density

myelin stripes ran majorly perpendicular to the V2 border (Fig. 7). This banded myelination pattern was very consistent across different scans and high test-retest reliability was observed in all hemispheres (Spearman correlation, $r_s > 0.8$, permutation test P -values $< 10^{-5}$) (Table 1). Interestingly, the heavily myelinated stripes are largely separate from color-selective thin stripes and disparity-selective thick stripes (clusters marked by blue and green dots, respectively), in each hemisphere and each subject (Fig. 8A). The interdigitating thin and thick stripes were located predominantly in low-myelination areas, again a result which is very consistent across monkeys. Given the interdigitating pattern of color-selective thin, disparity-selective thick and higher density myelin stripes, our data suggest that the latter correspond to the pale stripes (Roe et al. 2009).

To assess this result quantitatively, we performed a permutation test (see Materials and Methods) combining the data from the 2 hemispheres of each animal (Fig. 8B). In each animal, we found that the median myelin densities in both color (blue lines) and disparity stripes (green lines) was significantly lower than that observed in randomly selected vertices of V2d (P -values < 0.05). Hence, there is a significantly higher probability of finding color and disparity stripes in low-myelination areas of V2d, at least as assessed with (f)MRI.

The tSNR seemed to inversely covary with the myelin density within V2d (see Supplementary Fig. S2) as well. We found that the tSNR in V2d vertices excluding thin and thick stripes (i.e., interstripes) was significantly lower than the tSNR across the whole V2d in both the color and disparity stripe experiments (P -values $< 10^{-3}$, 100 000 permutations), after excluding vertices without enough tSNR (vertices with the 15% lowest tSNR values). Together with the results of Figure 8B, this probably reflects the inverse relationship between the T2* signal and the myelin density (Li et al. 2009; Chen et al. 2012).

However, tSNR is not a determinant factor for finding color and disparity stripes in lower myelinated areas. To prove this, we separated V2d into 10 equally spaced tSNR bands (excluding tSNR lower than the 15th percentile) and compared the median myelination values within each tSNR band. Across all tSNR bands and subjects, the median myelin density in color and disparity stripes were both significantly lower than the median myelin density in V2d vertices excluding color and disparity stripes (Wilcoxon signed-rank test, P -values < 0.04). No significant difference was observed between the median myelin density of color and disparity stripes, regardless of whether tSNR bands were selected based on data from the color or disparity experiment (Wilcoxon signed-rank test, P -values > 0.5). This result further confirmed the original permutation test, and suggests higher myelination in pale stripes.

Distance Between Stripes of Same Kind

As the local maximum of color- and disparity-selective activations most likely coincides with the centers of the respective stripes, the distance between nearest local maxima on the activation maps could be used to estimate the distance between stripes of the same kind. By drawing 20 lines distributed throughout the width of V2d and parallel to the V1d/V2d border, we calculated the median value of the distances along the cortical surface between all neighboring local maxima from the color- or disparity-selective activation maps. As the interstripe distances are not normally distributed (Jarque-Bera test), we used median and median absolute deviation (MAD) as robust statistical measurements. The estimated median distance between thin stripes is 4.02 mm (MAD = 0.93 mm) and between

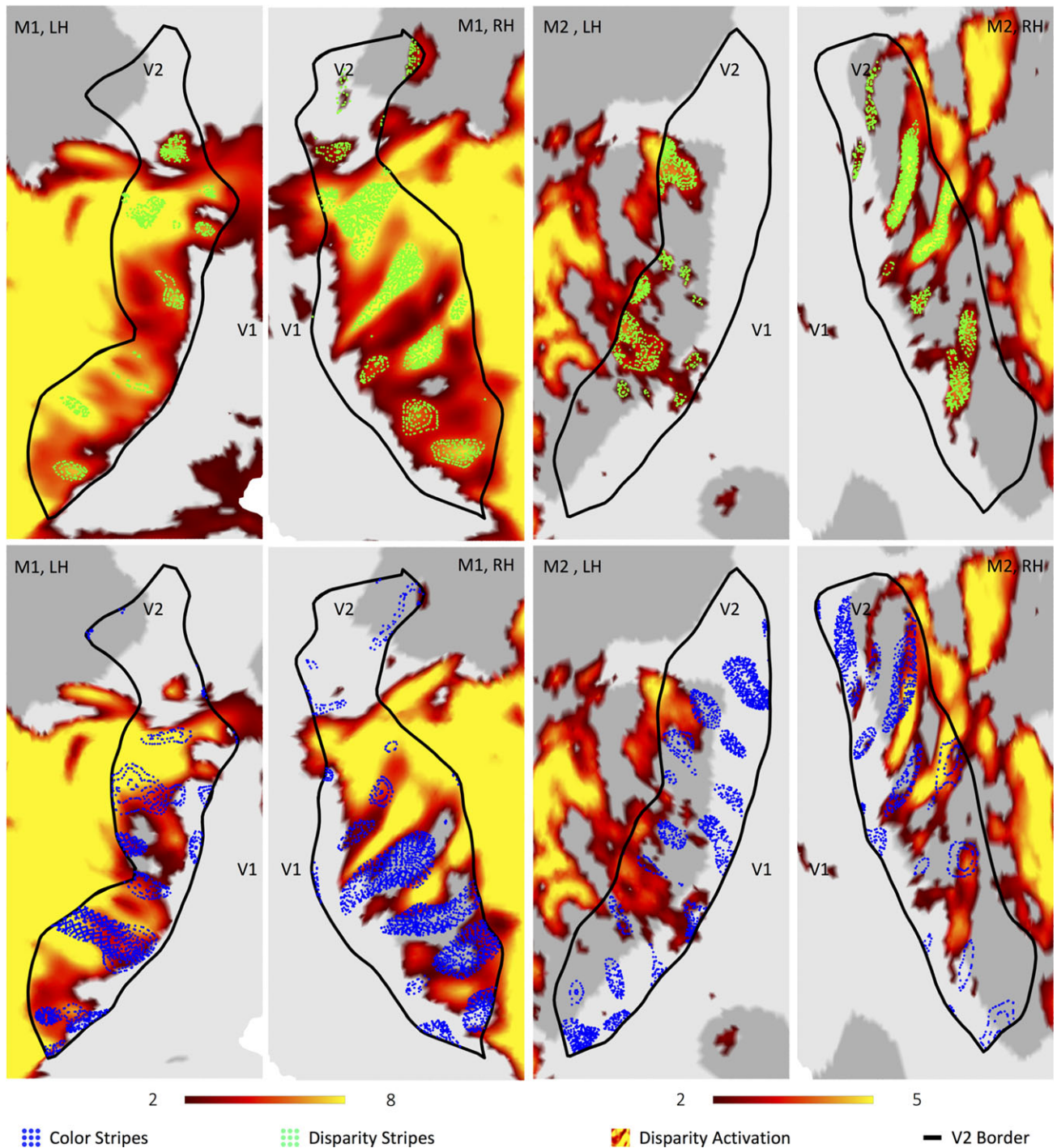


Figure 6. Disparity-selective activations and their relation to the thin (color-selective) stripes. Upper panels show disparity-selective activation maps. The functionally identified thick stripes are marked by green dots. Lower panels show co-registration of functionally defined thin stripes (marked by blue dots) and disparity-selective activation maps. They are largely separated from each other in every hemisphere of all the monkeys. Other details as in Figure 4.

thick stripes is 4.35 mm (MAD = 1.23 mm). There is no significant difference between the distances for thin and thick stripes ($P = 0.38$, Wilcoxon signed-rank test).

Discussion

The second visual area of primates (area V2) contains a repetitive pattern of 3 mesoscale elementary compartments: the thick

(disparity), thin (color), and pale stripes. However, due to their small size, they are only characterized by ex vivo approaches such as histology, or in vivo but invasive approaches, such as microelectrical recording or optical imaging in macaques. In this study, by combining high-resolution contrast agent enhanced fMRI with implanted phased-array coils, we were the first to demonstrate with MRI methods bands of color-selective activations interdigitating with disparity-selective activations

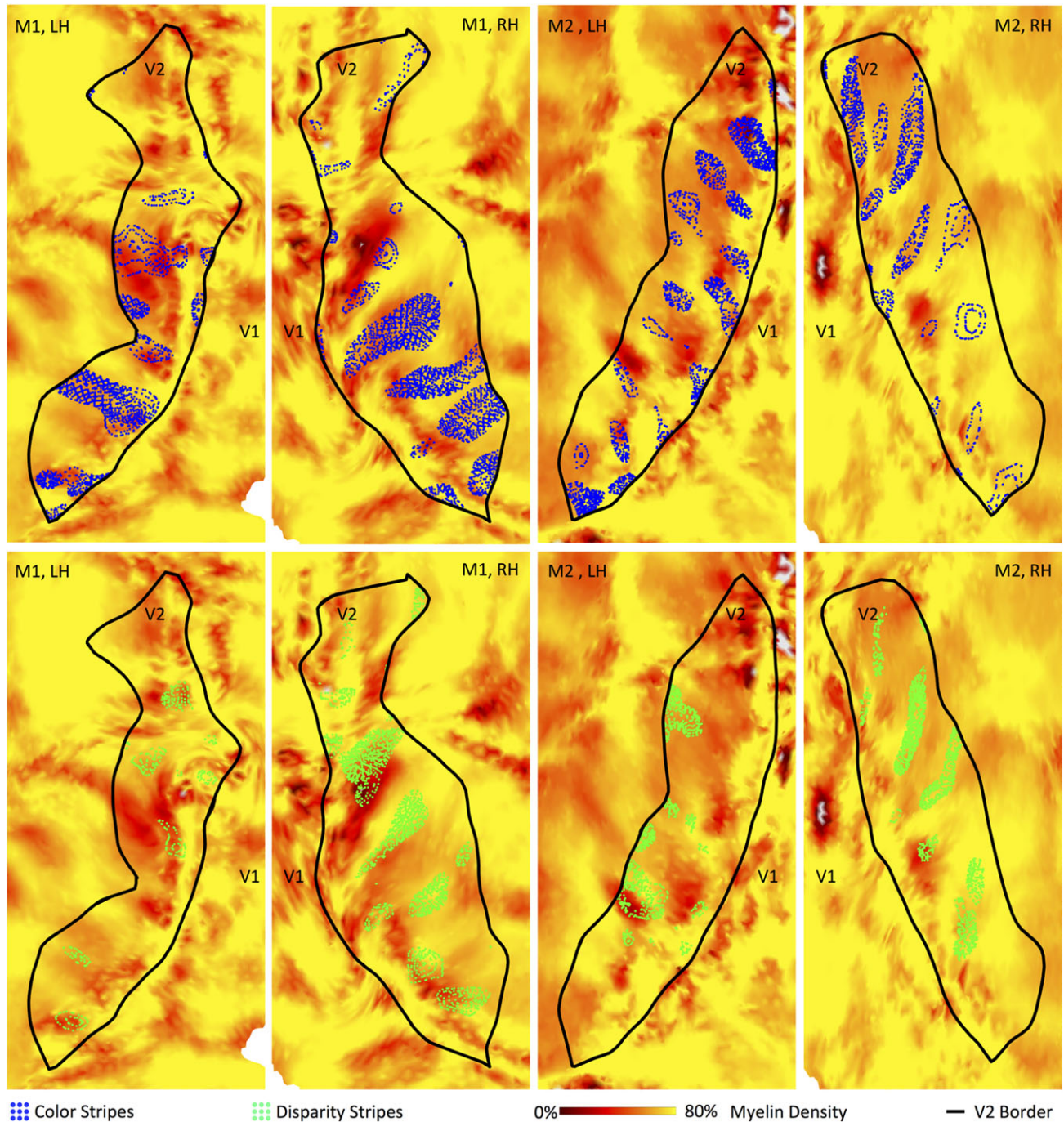


Figure 7. V2 myelin density maps from all hemispheres. The upper panels show co-registration of functionally defined thin stripes (marked by blue dots) and myelin density maps (heat maps). The lower panels show the co-registration of functionally defined thick stripes (marked by green dots) and myelin density maps. Other details as in Figure 4.

in retinotopically defined area V2d in monkeys. Moreover, *in vivo* MRI myelination mapping revealed that these 2 functionally defined stripe types are distinct from more highly myelinated stripe-like cortical zones. This interdigitating stripe pattern was highly reproducible across and within subjects. The data suggest that we can identify thick (disparity), thin (color), and pale (high myelination) stripes throughout V2d in monkeys, even using conventional 3 T scanners. In general, this approach clears the way for large-scale mesoscale functional imaging of the entire (extrastriate) cortex.

Comparison With fMRI-Defined V2-Stripes in Human

A recent human fMRI study showed an interdigitating pattern of disparity and color stripes (Nasr et al. 2016), very comparable to our results in the monkey. The distance between the human color stripes averaged 7.22 mm, while in the monkey this was 4.02 mm. For the thick stripes, these distances were 7.22 mm and 4.35 mm in human and monkey, respectively. These inter-stripe distances are also in accordance with the existing literature concerning monkey (Tootell and Hamilton 1989; Roe and

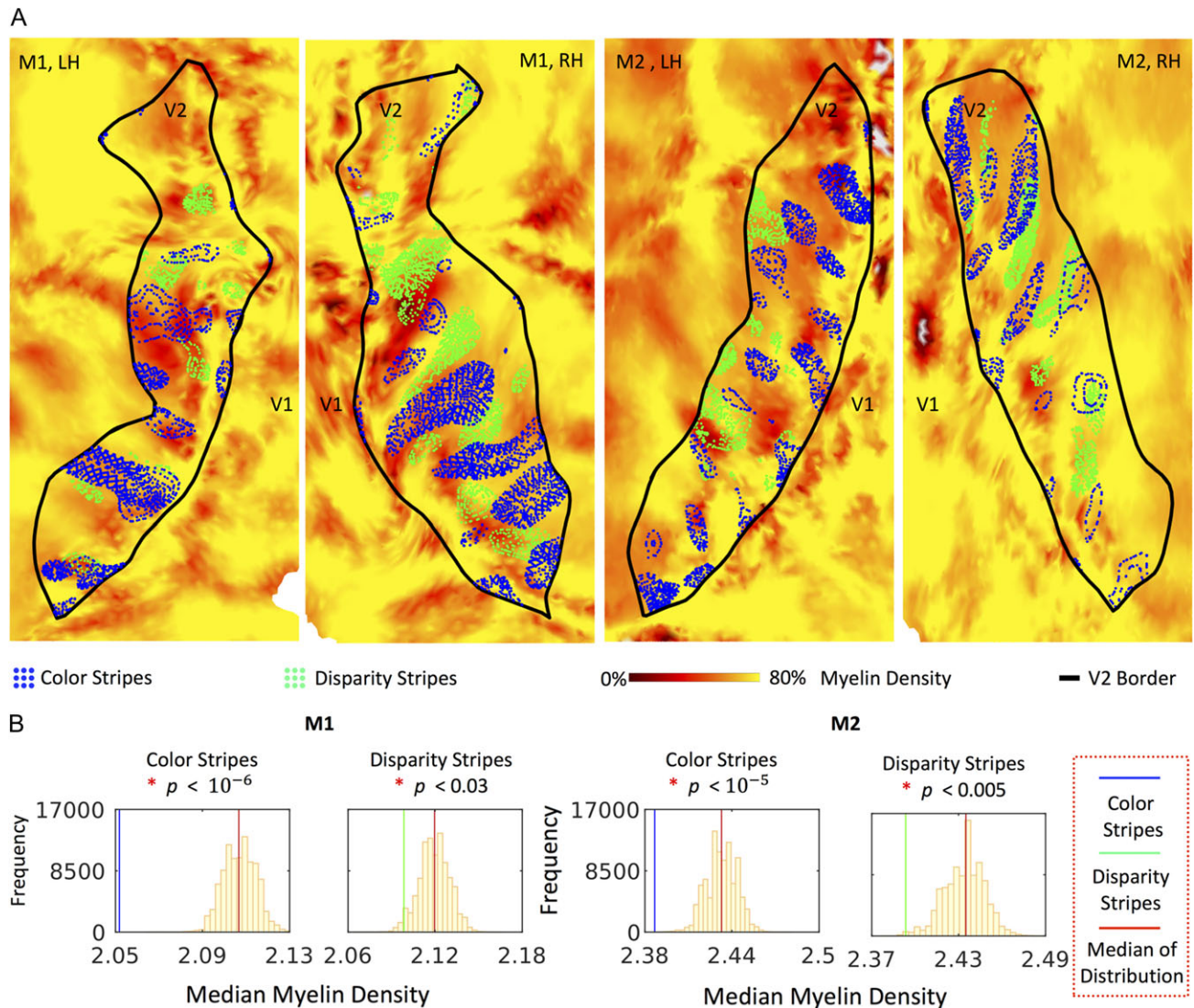


Figure 8. Comparison of myelin density maps with functionally defined thin and thick stripes. (A) Co-registration of functionally defined thin stripes (marked by blue dots), thick stripes (marked by green dots) and myelin density maps (heat maps). (B) Results of the permutation test comparing myelin density in thin and thick stripes with randomly selected vertices in V2d. The histograms indicate the distribution of the median myelin density from the randomly selected vertices. The median myelin density in the color and disparity stripes is indicated by blue and green vertical lines respectively and the median myelin density of the distribution is indicated by a red vertical line. The median myelin density in color and disparity stripes is significantly lower than the median myelin density in randomly selected vertices (P -values < 0.05 , 100 000 permutations) in each subject. Other details as in Figure 4.

Ts'o 1995, 1997; Lu et al. 2010) and human cortex (Hockfield et al. 1990; Tootell and Taylor 1995). Unlike the Nasr study, we made no attempt to measure stripe thickness based on fMRI data because width estimates are highly dependent upon the statistical thresholds used.

Another recent high-resolution human fMRI study (Dumoulin et al. 2017) used temporal frequency to distinguish 2 functional subdivisions within V2 which they attributed to motion-selective thick stripes versus a second compartment combining the thin and pale stripes. Their estimate of inter-stripe distance was 6 mm, slightly less than that of the Nasr et al. (2016)'s fMRI study and previous histological studies (Hockfield et al. 1990; Tootell and Taylor 1995) but still within the range of the 1.5/1 to 2/1 ratio between human and monkey interstripe distances (Tootell and Taylor 1995). In contrast to the present study, which provides strong quantitative evidence linking the regions with MRI-defined higher myelin density to

the putative pale stripes, Dumoulin et al. (2017) suggested that the more myelinated compartments in human V2 correspond to putative thick stripes as defined by high versus low temporal frequency. This conjecture was based mainly on the strong magnocellular input from layer 4B in V1 to the thick stripes in V2 (Livingstone and Hubel 1988; Sincich and Horton 2005). Contrasting activity evoked by high versus low temporal frequencies, however, may result in increased fMRI activity in not only the thick but also in pale stripes. Although direction of motion activates thick stripes as predicted by the connectivity (Roe et al. 2009; An et al. 2012), pale stripes are also activated by coherent motion (Peterhans and von der Heydt 1993) and axis of motion signals (An et al. 2012). Hence, the putative thick-stripes, as defined on the basis of temporal frequency in Dumoulin et al. (2017), may also include the neighboring pale stripe compartments. If this is the case, the 2 compartments reported in the Dumoulin study comprise the "thick and pale"

versus the “thin” stripes, instead of the “thick” versus the “thin and pale” stripes as they suggest. To rule out possible species differences and to resolve this question, future research will be required to determine whether the combination of functionally defined and T1- and T2-w measures of myelin stripes (for instance the putative pale stripes of the present experiment) correspond to some incontrovertible measure of myelin density in V2. Such a measurement will most likely require immunohistochemistry, given the conflicting results using different myelin staining methods in gray matter (Horton and Hocking 1997).

Large Draining Veins?

The previously mentioned V2-stripe study in humans (Nasr et al. 2016) showed that artefacts caused by draining veins can contribute to some patchy activations in the superficial layers. To mitigate this problem, these authors selected only data from the deeper V2 layers for subsequent analyses. Our use of the MION contrast agent to measure CBV changes, rather than BOLD signals, avoids these sorts of patchy vessel artefacts (Vanduffel et al. 2001; Leite et al. 2002; Zhao et al. 2006; Poplawsky and Kim 2014; Poplawsky et al. 2015). Furthermore, the widely separated color and disparity activations in V2 cannot be explained as vein-related artefacts, as in that case both would have to coincide with the locations of large veins.

Subcompartments Within Single Stripes

Although V2 is characterized by a banded pattern with each stripe type housing neurons with different selectivities, individual stripes are not uniform with respect to functional properties or connectivity. Stripes contain even smaller subcompartments, measuring only about 0.5 mm in diameter and have been observed in 2L-DG (Vanduffel et al. 2002; Tootell et al. 2004), optical imaging (Roe and Ts'o 1995; Ts'o et al. 2001; Chen et al. 2008; An et al. 2012) and anatomical pathway tracing studies (DeYoe et al. 1994). For example, single-unit recordings from 2 neighboring subcompartments within a single thin stripe showed either color- or luminance-selectivities in different subregions (Ts'o et al. 2001). These subcompartments may be visible in our results, since the fMRI-defined stripes typically showed the discontinuities and irregularities also observed in the Nasr et al. (2016) and Dumoulin et al. (2017) human fMRI studies. However, it is likely that we are unable to distinguish all subcompartments due to potential partial volume effects.

Mixed Selectivities at Stripe Borders

In some hemispheres, we observed a small but consistent overlap between color and disparity-selective regions (e.g., in the right hemisphere of M2, see Fig. 8A). This is consistent with previous findings showing that some cells are selective for both color and disparity at the borders between stripes (Roe and Ts'o 1995; Ts'o et al. 2001), despite the largely separated pathways for color and disparity in V2. This apparent overlap may also be related to the statistical thresholds inherent to the fMRI analyses used.

Weak Color-Selective Activation in Thick/Pale Stripes?

In our previous 2L-DG study (Tootell et al. 2004), a very weak luminance-biased activation was found in the thick and inter-stripes, while in current study we sometimes observed color-biased activity in these stripes. This discrepancy may be caused

by the imperfect iso-luminance ratio used for the color grating stimuli. In the 2L-DG study (Tootell et al. 2004), a subject-specific iso-luminance ratio between red and blue colors was measured based on the visual evoked potential (VEP) response of the primary visual cortex for each monkey separately and the ratios varied from 5.33 to 6.24 in 3 monkeys, whereas in our study we took the group-average ratio (i.e., 6) from the 2L-DG study. We also did not vary the luminance ratios as function of eccentricity, which would better reflect the varying cone distributions across the retina (Mullen 1985; Livingstone and Hubel 1987). Therefore, it is possible that the luminance was slightly mismatched in our color stimuli at the subject-level, which biased the slight negative color-biased responses that were originally observed by Tootell et al. (2004) towards slightly positive in our experiment.

Missing Stripes

The iso-luminance ratio of color-varying stimuli is also eccentricity-dependent in both macaque (Mullen 1985; Livingstone and Hubel 1987) and human (Tootell et al. 1983; Bilodeau and Faubert 1997) and varies extensively among individuals. Hence, the fixed iso-luminance ratio used in our experiment may have slightly deviated from physiological and psychophysical iso-luminance at some or all eccentricities. Given the fixed spatial frequency of the stimuli used and the eccentricity-dependent frequency tuning of V2 (Foster et al. 1985), these factors may explain the inhomogeneous color and disparity selectivity observed across the extent of V2d (i.e., stripes not detectable throughout all of V2d).

Although some stripes might have been missed, the general pattern of the different stripes and the distances between them are consistent with previous studies. To further confirm our results, postmortem immunocytochemistry would be useful to compare CO or myelin-defined stripes with the in vivo MRI results.

Future for High-Resolution fMRI on Awake Monkey

By confirming that all 3 types of V2 stripes can be detected, our results indicate that submillimeter scale (f)MRI can be reliably used to study mesoscopic-scale brain structures in macaque monkeys, even at 3 T. Combining the present technology with super-high-field scanners (7 T and higher) and optimized coils (implanted, external or a combination) that improve the sensitivity of the ventral areas offers great potential to investigate yet finer-scale functional organizations, even in far extrastriate cortex such as inferotemporal cortex where accessibility is difficult or impossible using microscope-dependent imaging tools (Tanaka 2003). In such a case, improved motion reduction or motion/susceptibility correction methods may become more critical to handle susceptibility artifacts introduced by monkeys that move their unconstrained bodies during the fMRI sessions.

Supplementary Material

Supplementary data are available at *Cerebral Cortex* online.

Funding

Inter-University Attraction Pole 7/11, the Research Foundation Flanders (FWO-Flanders) (G0B8617N, G0A5613N and Odysseus G0007.12); KU Leuven Programme Financing (PFV/10/008 and C14/17/109); European Union's Horizon 2020 Framework Programme for Research and Innovation under Grant Agreement No. 720270 (Human Brain Project SGA1), and the

Hercules foundation. Q.Z and J.A. are postdoctoral fellows of the FWO-Flanders.

Notes

The authors thank A. Coeman, C. Fransen, P. Kayenbergh, I. Puttemans, S. De Pril, A. Hermans, G. Meulemans, W. Depuydt, C. Ulens, S. Verstraeten, and M. Depaep for technical and administrative support. We are indebted to J. Polimeni and T. Witzel for their assistance in fine-tuning the high-resolution MR-sequences. The authors also thank S. Raiguel for his comments on the article. *Conflict of Interest*: None declared.

References

- An X, Gong H, Qian L, Wang X, Pan Y, Zhang X, Yang Y, Wang W. 2012. Distinct functional organizations for processing different motion signals in V1, V2, and V4 of macaque. *J Neurosci*. 32:13363–13379.
- Angelucci A, Rosa MGP. 2015. Resolving the organization of the third tier visual cortex in primates: a hypothesis-based approach. *Vis Neurosci*. 32:E010.
- Bilodeau L, Faubert J. 1997. Isoluminance and chromatic motion perception throughout the visual field. *Vision Res*. 37:2073–2081.
- Chau BKH, Sallet J, Papageorgiou GK, Noonan MAP, Bell AH, Walton ME, Rushworth MFS. 2015. Contrasting roles for orbitofrontal cortex and amygdala in credit assignment and learning in macaques. *Neuron*. 87:1106–1118.
- Chen G, Lu HD, Roe AW. 2008. A map for horizontal disparity in monkey V2. *Neuron*. 58:442–450.
- Chen G, Wang F, Gore JC, Roe AW. 2012. Identification of cortical lamination in awake monkeys by high resolution magnetic resonance imaging. *Neuroimage*. 59:3441–3449.
- Chung M, Hartley R, Dalton KM, Davidson RJ. 2008. Encoding cortical surface by spherical harmonics. *Stat Sin*. 18:1269–1291.
- Dale AM, Fischl B, Sereno MI. 1999. Cortical surface-based analysis: I. Segmentation and surface reconstruction. *Neuroimage*. 9:179–194.
- De Martino F, Moerel M, Xu J, Van De Moortele PF, Ugurbil K, Goebel R, Yacoub E, Formisano E. 2015. High-resolution mapping of myeloarchitecture in vivo: localization of auditory areas in the human brain. *Cereb Cortex*. 25:3394–3405.
- De Martino F, Zimmermann J, Muckli L, Ugurbil K, Yacoub E, Goebel R. 2013. Cortical depth dependent functional responses in humans at 7T: improved specificity with 3D GRASE. *PLoS One*. 8:e60514.
- DeYoe EA, Felleman DJ, Van Essen DC, McClendon E. 1994. Multiple processing streams in occipitotemporal visual cortex. *Nature*. 371:151–154.
- DeYoe EA, Van Essen DC. 1985. Segregation of efferent connections and receptive field properties in visual area V2 of the macaque. *Nature*. 317:58–61.
- Dumoulin SO, Harvey BM, Fracasso A, Zuiderbaan W, Luijten PR, Wandell BA, Petridou N. 2017. In vivo evidence of functional and anatomical stripe-based subdivisions in human V2 and V3. *Sci Rep*. 7:733.
- Fischl B, Sereno MI, Dale AM. 1999. Cortical surface-based analysis: II: Inflation, flattening, and a surface-based coordinate system. *Neuroimage*. 9:195–207.
- Fischl B, Sereno MI, Tootell RBH, Dale AM. 1999. High-resolution inter-subject averaging and a surface-based coordinate system. *Hum Brain Mapp*. 8:272–284.
- Foster KH, Gaska JP, Nagler M, Pollen DA. 1985. Spatial and temporal frequency selectivity of neurones in visual cortical areas V1 and V2 of the macaque monkey. *J Physiol*. 365:331–363.
- Fracasso A, Van Veluw SJ, Visser F, Luijten PR, Spliet W, Zwanenburg JJM, Dumoulin SO, Petridou N. 2016. Lines of Baillarger in vivo and ex vivo: myelin contrast across lamina at 7 T MRI and histology. *Neuroimage*. 133:163–175.
- Fukuda M, Moon CH, Wang P, Kim SG. 2006. Mapping iso-orientation columns by contrast agent-enhanced functional magnetic resonance imaging: reproducibility, specificity, and evaluation by optical imaging of intrinsic signal. *J Neurosci*. 26:11821–11832.
- Gattass R, Gross CG, Sandell JH. 1981. Visual topography of V2 in the macaque. *J Comp Neurol*. 201:519–539.
- Gattass R, Lima B, Soares JGM, Ungerleider LG. 2015. Controversies about the visual areas located at the anterior border of area V2 in primates. *Vis Neurosci*. 32:E019.
- Gattass R, Sousa A, Gross CG. 1988. Visuotopic organization and extent of V3 and V4 of the macaque. *J Neurosci*. 8:1831–1845.
- Geyer S, Weiss M, Reimann K, Lohmann G, Turner R. 2011. Microstructural parcellation of the human cerebral cortex: from Brodmann's post-mortem map to in vivo mapping with high-field magnetic resonance imaging. *Front Hum Neurosci*. 5:19.
- Glasser MF, Goyal MS, Preuss TM, Raichle ME, Van Essen DC. 2014. Trends and properties of human cerebral cortex: correlations with cortical myelin content. *Neuroimage*. 93:165–175.
- Glasser MF, Sotiropoulos SN, Wilson JA, Coalson TS, Fischl B, Andersson JL, Xu J, Jbabdi S, Webster M, Polimeni JR, et al. 2013. The minimal preprocessing pipelines for the Human Connectome Project. *Neuroimage*. 80:105–124.
- Glasser MF, Van Essen DC. 2011. Mapping human cortical areas in vivo based on myelin content as revealed by T1- and T2-weighted MRI. *J Neurosci*. 31:11597–11616.
- Harel N, Lin J, Moeller S, Ugurbil K, Yacoub E. 2006. Combined imaging-histological study of cortical laminar specificity of fMRI signals. *Neuroimage*. 29:879–887.
- Hockfield S, Tootell RB, Zaremba S. 1990. Molecular differences among neurons reveal an organization of human visual cortex. *Proc Natl Acad Sci USA*. 87:3027–3031.
- Hoge WS, Polimeni JR. 2015. A dual-polarity GRAPPA kernel for the robust reconstruction of accelerated EPI data. In: *Proceedings of International Symposium on Biomedical Imaging*. pp. 1244–1247.
- Horton JC. 1984. Cytochrome oxidase patches: a new cytoarchitectonic feature of monkey visual cortex. *Philos Trans R Soc Lond B Biol Sci*. 304:199–253.
- Horton JC, Hocking DR. 1997. Myelin patterns in V1 and V2 of normal and monocularly enucleated monkeys. *Cereb Cortex*. 7:166–177.
- Janssens T, Keil B, Farivar R, McNab JA, Polimeni JR, Gerits A, Arsenault JT, Wald LL, Vanduffel W. 2012. An implanted 8-channel array coil for high-resolution macaque MRI at 3T. *Neuroimage*. 62:1529–1536.
- Janssens T, Zhu Q, Popivanov ID, Vanduffel W. 2014. Probabilistic and single-subject retinotopic maps reveal the topographic organization of face patches in the macaque cortex. *J Neurosci*. 34:10156–10167.

- Jefferies J, Federe F, Angelucci A. 2015. Corticocortical connection patterns reveal two distinct visual cortical areas bordering dorsal V2 in marmoset monkey. *Vis Neurosci*. 32:E012.
- Jefferies J, Federer F, Ichida JM, Angelucci A. 2013. High-resolution mapping of anatomical connections in marmoset extrastriate cortex reveals a complete representation of the visual field bordering dorsal V2. *Cereb Cortex*. 23:1126–1147.
- Jefferies J, Ichida JM, Federer F, Angelucci A. 2009. Anatomical evidence for classical and extra-classical receptive field completion across the discontinuous horizontal meridian representation of primate area V2. *Cereb Cortex*. 19:963–981.
- Jenkinson M, Beckmann CF, Behrens TEJ, Woolrich MW, Smith SM. 2012. FSL. *Neuroimage*. 62:782–790.
- Jezzard P, Balaban RS. 1995. Correction for geometric distortion in echo planar images from B0 field variations. *Magn Reson Med*. 34:65–73.
- Jovicich J, Czanner S, Greve D, Haley E, Van Der Kouwe A, Gollub R, Kennedy D, Schmitt F, Brown G, MacFall J, et al. 2006. Reliability in multi-site structural MRI studies: effects of gradient non-linearity correction on phantom and human data. *Neuroimage*. 30:436–443.
- Kaas JH, Roe AW, Baldwin MKL, Lyon DC. 2015. Resolving the organization of the territory of the third visual area: a new proposal. *Vis Neurosci*. 32:E016.
- Kay KN, Rokem A, Winawer J, Dougherty RF, Wandell BA. 2013. GLMdenoise: a fast, automated technique for denoising task-based fMRI data. *Front Neurosci*. 7:1–15.
- Kemper VG, De Martino F, Yacoub E, Goebel R. 2016. Variable flip angle 3D-GRASE for high resolution fMRI at 7 tesla. *Magn Reson Med*. 76:897–904.
- Kim T, Kim SG. 2010. Cortical layer-dependent arterial blood volume changes: improved spatial specificity relative to BOLD fMRI. *Neuroimage*. 49:1340–1349.
- Kim T, Zhao T, Bae KT. 2016. Enhancement of functional MRI signal at high-susceptibility regions of brain using simultaneous multiecho multithin-slice summation imaging technique. *J Magn Reson Imaging*. 44:478–485.
- Kolster H, Mandeville JB, Arsenault JT, Ekstrom LB, Wald LL, Vanduffel W. 2009. Visual field map clusters in macaque extrastriate visual cortex. *J Neurosci*. 29:7031–7039.
- Krubitzer L, Kaas J. 1989. Cortical integration of parallel pathway in the visual system of primates. *Brain Res*. 478:161–165.
- Leite FP, Tsao D, Vanduffel W, Fize D, Sasaki Y, Wald LL, Dale AM, Kwong KK, Orban GA, Rosen BR, et al. 2002. Repeated fMRI using iron oxide contrast agent in awake, behaving macaques at 3 Tesla. *Neuroimage*. 16:283–294.
- Levitt JB, Kiper DC, Movshon JA. 1994. Receptive fields and functional architecture of macaque V2. *J Neurophysiol*. 71:2517–2542.
- Li T-Q, Yao B, van Gelderen P, Merkle H, Dodd S, Talagala L, Koretsky AP, Duyn J. 2009. Characterization of T(2)* heterogeneity in human brain white matter. *Magn Reson Med*. 62:1652–1657.
- Liu N, Hadj-Bouziane F, Jones KB, Turchi JN, Averbeck BB, Ungerleider LG. 2015. Oxytocin modulates fMRI responses to facial expression in macaques. *Proc Natl Acad Sci USA*. 112:E3123–E3130.
- Livingstone MS, Hubel DH. 1987. Psychophysical evidence for separate channels for the perception of form, color, movement, and depth. *J Neurosci*. 7:3416–3468.
- Livingstone M, Hubel D. 1988. Segregation of form, color, movement, and depth: anatomy, physiology, and perception. *Science*. 240:740–749.
- Lu HD, Chen G, Tanigawa H, Roe AW. 2010. A motion direction map in macaque V2. *Neuron*. 68:1002–1013.
- Lyon D, Liu Y, Arreola M, Coleman C. 2014. Very-long-range synaptic V1 connections through layer 6 pyramidal neurons revealed by transneuronal tracing with rabies virus. *Eye Brain*. 6:45–46.
- Miyamoto K, Osada T, Setsuie R, Takeda M, Tamura K, Adachi Y, Miyashita Y. 2017. Causal neural network of metamemory for retrospection in primates. *Science*. 355:188–193.
- Moeller S, Crapse T, Chang L, Tsao DY. 2017. The effect of face patch microstimulation on perception of faces and objects. *Nat Neurosci*. 20:743–752.
- Muckli L, De Martino F, Vizioli L, Petro LS, Smith FW, Ugurbil K, Goebel R, Yacoub E. 2015. Contextual feedback to superficial layers of V1. *Curr Biol*. 25:2690–2695.
- Mullen KT. 1985. The contrast sensitivity of human colour vision to red-green and blue-yellow chromatic gratings. *J Physiol*. 359:381–400.
- Nasr S, Polimeni JR, Tootell RBH. 2016. Interdigitated color- and disparity-selective columns within human visual cortical areas V2 and V3. *J Neurosci*. 36:1841–1857.
- Nunes RG, Hajnal JV, Golay X, Larkman DJ. 2006. Simultaneous slice excitation and reconstruction for single shot EPI. *Proc Intl Soc Mag Reson Med*. 14:293.
- Peterhans E, von der Heydt R. 1993. Functional organization of area V2 in the alert macaque. *Eur J Neurosci*. 5:509–524.
- Poplawsky AJ, Fukuda M, Murphy M, Kim S-G. 2015. Layer-specific fMRI responses to excitatory and inhibitory neuronal activities in the olfactory bulb. *J Neurosci*. 35:15263–15275.
- Poplawsky AJ, Kim SG. 2014. Layer-dependent BOLD and CBV-weighted fMRI responses in the rat olfactory bulb. *Neuroimage*. 91:237–251.
- Reithler J, Peters JC, Goebel R. 2017. Characterizing object- and position-dependent response profiles to uni- and bilateral stimulus configurations in human higher visual cortex: a 7T fMRI study. *Neuroimage*. 152:551–562.
- Roe AW, Chen LM. 2008. High-resolution fMRI maps of cortical activation in nonhuman primates: correlation with intrinsic signal optical images. *ILAR J*. 49:116–123.
- Roe AW, Chen G, Lu HD. 2009. Visual system: functional architecture of area V2. *Encyclopedia of Neuroscience*. In: Oxford (UK). Elsevier Ltd.
- Roe AW, Ts'o DY. 1995. Visual topography in primate V2—multiple representation across functional stripes. *J Neurosci*. 15:3689–3715.
- Roe AW, Ts'o DY. 1997. The functional architecture of area V2 in the macaque monkey: physiology, topography, and connectivity, cerebral cortex. New York: Plenum Press.
- Rosa MGP, Angelucci A, Jeffers J, Pettigrew JD. 2013. The case for a dorsomedial area in the primate “third-tier” visual cortex. *Proc Biol Sci*. 280:20121372. discussion 20121994.
- Rosa MGP, Palmer SM, Gamberini M, Burman KJ, Yu H-H, Reser DH, Bourne JA, Tweedale R, Galletti C. 2009. Connections of the dorsomedial visual area: pathways for early integration of dorsal and ventral streams in extrastriate cortex. *J Neurosci*. 29:4548–4563.
- Rosa MGP, Palmer SM, Gamberini M, Tweedale R, Pi On MC, Bourne JA. 2005. Resolving the organization of the new world monkey third visual complex: the dorsal extrastriate cortex of the marmoset (*Callithrix jacchus*). *J Comp Neurol*. 483:164–191.
- Rosa MGP, Tweedale R. 2000. Visual areas in lateral and ventral extrastriate cortices of the marmoset monkey. *J Comp Neurol*. 422:621–651.

- Russ BE, Kaneko T, Saleem KS, Berman RA, Leopold DA. 2016. Distinct fMRI responses to self-induced versus stimulus motion during free viewing in the macaque. *J Neurosci.* 36: 9580–9589.
- Sereno M, Dale A, Reppas J, Kwong K, Belliveau J, Brady T, Rosen B, Tootell R. 1995. Borders of multiple visual areas in humans revealed by functional magnetic resonance imaging. *Science.* 268:889–893.
- Sereno MI, Lutti A, Weiskopf N, Dick F. 2013. Mapping the human cortical surface by combining quantitative T1 with retinotopy. *Cereb Cortex.* 23:2261–2268.
- Sereno MI, McDonald CT, Allman JM. 2015. Retinotopic organization of extrastriate cortex in the owl monkey—dorsal and lateral areas. *Vis Neurosci.* 32:E021.
- Sincich LC, Horton JC. 2005. The circuitry of V1 and V2: integration of color, form, and motion. *Annu Rev Neurosci.* 28: 303–326.
- Sliwa J, Freiwald WA. 2017. A dedicated network for social interaction processing in the primate brain. *Science.* 749: 745–749.
- Tanaka K. 2003. Columns for complex visual object features in the inferotemporal cortex: clustering of cells with similar but slightly different stimulus selectivities. *Cereb Cortex.* 13: 90–99.
- Thorell LG, DeValois RL, Albrecht DF. 1984. Spatial mapping of monkey V1 cells with pure color and luminance stimuli. *Vision Res.* 24:751–769.
- Tootell RB, Hamilton SL. 1989. Functional anatomy of the second visual area (V2) in the macaque. *J Neurosci.* 9:2620–2644.
- Tootell RBH, Nelissen K, Vanduffel W, Orban GA. 2004. Search for color “center(s)” in macaque visual cortex. *Cereb Cortex.* 14:353–363.
- Tootell RB, Silverman MS, De Valois RL, Jacobs GH. 1983. Functional organization of the second cortical visual area in primates. *Science.* 220:737–739.
- Tootell RBH, Taylor JB. 1995. Anatomical evidence for MT and additional cortical visual areas in humans. *Cereb Cortex.* 5: 39–55.
- Ts'o DY, Roe AW, Gilbert CD. 2001. A hierarchy of the functional organization for color, form and disparity in primate visual area V2. *Vision Res.* 41:1333–1349.
- Van Essen DC, Drury H a., Dickson J, Harwell J, Hanlon D, Anderson CH. 2001. An integrated software suite for surface-based analyses of cerebral cortex. *J Am Med Inform Assoc.* 8:443–459.
- Vanduffel W, Fize D, Mandeville JB, Nelissen K, Van Hecke P, Rosen BR, Tootell RBH, Orban GA. 2001. Visual motion processing investigated using contrast agent-enhanced fMRI in awake behaving monkeys. *Neuron.* 32:565–577.
- Vanduffel W, Tootell RBH, Schoups AA, Orban GA. 2002. The organization of orientation selectivity throughout macaque visual cortex. *Cereb Cortex.* 12:647–662.
- Wang Z, Chen LM, Négyessy L, Friedman RM, Mishra A, Gore JC, Roe AW. 2013. The relationship of anatomical and functional connectivity to resting-state connectivity in primate somatosensory cortex. *Neuron.* 78:1116–1126.
- Xu J, Moeller S, Auerbach EJ, Strupp J, Smith SM, Feinberg DA, Yacoub E, Uğurbil K. 2013. Evaluation of slice accelerations using multiband echo planar imaging at 3T. *Neuroimage.* 83: 991–1001.
- Yacoub E, Harel N, Uğurbil K. 2008. High-field fMRI unveils orientation columns in humans. *Proc Natl Acad Sci USA.* 105: 10607–10612.
- Yue X, Pourladian IS, Tootell RBH, Ungerleider LG. 2014. Curvature-processing network in macaque visual cortex. *Proc Natl Acad Sci USA.* 111:E3467–E3475.
- Zhao F, Wang P, Hendrich K, Kim SG. 2005. Spatial specificity of cerebral blood volume-weighted fMRI responses at columnar resolution. *Neuroimage.* 27:416–424.
- Zhao F, Wang P, Hendrich K, Uğurbil K, Kim SG. 2006. Cortical layer-dependent BOLD and CBV responses measured by spin-echo and gradient-echo fMRI: insights into hemodynamic regulation. *Neuroimage.* 30:1149–1160.
- Zhu Q, Nelissen K, Van den Stock J, De Winter F-L, Pauwels K, de Gelder B, Vanduffel W, Vandenbulcke M. 2012. Dissimilar processing of emotional facial expressions in human and monkey temporal cortex. *Neuroimage.* 66C:402–411.
- Zimmermann J, Goebel R, de Martino F, van de Moortele PF, Feinberg D, Adriany G, Chaimow D, Shmuel A, Uğurbil K, Yacoub E. 2011. Mapping the organization of axis of motion selective features in human area MT using high-field fMRI. *PLoS One.* 6:e28716.